Fast Method for Correcting Image Misregistration Due to Organ Motion in Time-Series MRI Data

Sandeep N. Gupta,[1*] Meiyappan Solaiyappan,[2] Garth M. Beache,[3] Andrew E. Arai,[4] and Thomas K.F. Foo[1]

Time-series MRI data often suffers from image misalignment due to patient movement and respiratory and other physiologic motion during the acquisition process. It is necessary that this misalignment be corrected prior to any automated quantitative analysis. In this article a fast and automated technique for removing in-plane misalignment from time-series MRI data is presented. The method is computationally efficient, robust, and fine-tuned for the clinical setting. The method was implemented and tested on data from 21 human subjects, including myocardial perfusion imaging, renal perfusion imaging, and blood-oxygen level-dependent cardiac T_2^* imaging. In these applications 10-fold or better reduction in image misalignment is reported. The improvement after registration on representative time–intensity curves is shown. Although the method currently corrects translation motion using image center of mass, the mathematical framework of our approach may be extended to correct rotation and other higher-order displacements. Magn Reson Med 49:506–514, 2003. © 2003 Wiley-Liss, Inc.

Key words: image registration; motion correction; perfusion imaging; BOLD imaging

Image misalignment due to gross motion is a common problem in clinical applications that involve time-series data. In these applications, improving the acquisition techniques, for example, by ultrafast imaging to limit cardiac and respiratory motion, can optimize the quality of each image, but their usefulness is still limited as a time-series due to frame-to-frame motion occurring during the total acquisition. An example of this occurs in myocardial perfusion imaging using MRI, where the goal is to characterize the abnormal distribution of myocardial blood flow using the infusion of paramagnetic contrast agents (1,2). Image analysis of perfusion images aims to construct representative time–intensity curves from specified regions of interest and quantitative parametric maps indexing physiological parameters (3). The automatic computation of these curves is complicated when patients do not breathhold adequately, resulting in image misalignment over time. This occurs frequently because first-pass transit of contrast agents is typically imaged over 30–60 sec, which is too long for a breathhold. Thus, in perfusion imaging and other such applications, it becomes imperative to correct the misalignment of the images by registering them prior to their use for quantification.

Registration remains an area of active investigation in image processing with applications in several fields (4–11), including MRI (12–15). The early 1960s witnessed pioneering works in this field inspired by the application of mathematical theories on functions of variables to images. The need for highly efficient image processing algorithms led to the development of novel approaches where computers were extensively used for target recognition and tracking. Among them, two principles are of utmost value to the design of an efficient approach for registering time-series image data:

1) Determining the mutual correspondence between a pair of successive images in a time-series.
2) Identifying the properties of the data that are invariant under transformations such as translation or rotation.

Methods based on the first principle frequently use correlation as a measure of the associativity between functions and then find the location of maximum correlation (16). This approach has been widely used to solve registration problems in medical imaging such as 3D reconstructions from autoradiograms (17) and histological sections (18), multimodality registration (19,20), and 3D spatial alignment (21). However, application of cross-correlation to image registration requires additional considerations. This is due to the fact that the correlation may be too broad and finding a peak in the correlation may be difficult (22). Further, 2D image registration is computationally intensive, with a quadratic overhead with respect to size of the image (23). Thus, improving the performance by optimizing the correlation computations without sacrificing accuracy becomes key to an effective implementation of registration. In a recent work (24), the effectiveness of three different registration methods for motion correction in dynamic MRI of the kidneys was compared. The authors found that a Fourier-based approach measuring the phase-differences between images yielded better performance than image matching using cross-correlation. This can be attributed to the fact that the correlation can be influenced by incorrect local maxima during a global search. But Fourier-based approaches have the limitation of requiring image prefiltering to minimize the influence of sharp edges.

In contrast, methods based on the second principle were motivated by classical mechanics. Dealing with objects that extend spatially in two and three dimensions, the notions of center of mass and moments were developed to

[1]Applied Sciences Laboratory, GE Medical Systems, Baltimore, Maryland.
[2]Department of Radiology, Johns Hopkins School of Medicine, Baltimore, Maryland.
[3]Cardiovascular Imaging and Physiology Center, Department of Radiology, University of Maryland Medical Center, Baltimore, Maryland.
[4]Laboratory of Cardiac Energetics, NHLBI, National Institutes of Health, Bethesda, Maryland.
*Correspondence to: Sandeep N. Gupta, GE Medical Systems, Johns Hopkins Hospital, Room MRI 110, 600 N. Wolfe Street, Baltimore, MD 21287. E-mail: Sandeep.Gupta@med.ge.com
Received 4 January 2002; revised 15 October 2002; accepted 17 October 2002.
DOI 10.1002/mrm.10394
Published online in Wiley InterScience (www.interscience.wiley.com).

study their rigid body motions under external forces. The mathematical properties of moments made them ideal for studying statistical functions. Moments are used to measure uniqueness and invariance under transformation of the distribution. Images as a distribution of pixel samples can be regarded as a 2D probability distribution function. Thus, Hu (25) showed that moments can be used for recognizing images and classifying them independent of their 2D spatial orientations. Pitts and McCulloch (26) suggested that our visual nervous system could plausibly use the center of mass of an image to produce necessary oculomotor reflexes to converge the two eyes on a target when it is in motion.

In our proposed approach, the two principles were combined to create a clinically usable methodology specific to MR images without the individual shortcomings of either approach. For instance, the center of mass provides exact information regarding the translation of a rigid object. Thus, in principle (for a binary image), this should be sufficient to compute the registration. However, small shape changes in the images, as would happen when imaging moving organs of interest, could be sufficient to make the results inaccurate. But the results can still be used to yield an approximate estimate of the displacement. Likewise, the registration process using correlation consumes considerable time to process a pair of images due to the iterative nature of the solution, although the results may be more accurate. Thus, by using the center of mass as an initial guess followed by registration by correlation provides a method that has the benefits of both. Further, since the correlation search is restricted to a region around the center of mass guess, the result is more robust than a global search.

We demonstrate the application of this approach for registering time-series data from first-pass perfusion imaging of the heart and kidneys and from myocardial BOLD imaging.

MATERIALS AND METHODS

In applications where the organs being imaged do not undergo significant elastic deformation or rotations, it is simple and efficient to correct the translational motion using rigid body registration methods. Although translation registration is relatively simpler than elastic or general rigid body registration techniques, the size of the images and the number of images that need to be registered demands more efficient implementation than that found in routine pattern matching algorithms.

In typical MRI applications, the spatial extent of an image field-of-view is much larger than the organ of interest due to signal/noise and aliasing considerations. As a result, the image includes surrounding structures, which may or may not have motion similar to the organ of interest. These surrounding structures impact the accuracy of the registration. The best global registration for the image as a whole may be different from the desired local registration of the region of interest. Thus, limiting the region that will be used for registration helps to eliminate the interference from surrounding structures. Furthermore, this increases the efficiency of the registration by restricting the computation to the desired part of the image.

Additionally, in perfusion images pixels undergo interframe intensity variations due to the transit of the contrast agent. Registration methods are very sensitive to these changes and suffer from errors in establishing pixel-correspondence between successive images in this situation. This requires a preliminary step of normalization of the images prior to registration. Considering the processing overhead, we implemented a simple threshold-based normalization technique, which is easy to compute. This produces a binary map of the organ and simplifies the subsequent correlation calculation.

Before registering the binary maps of the images, we consider the following simplification. Consider an image feature represented by a pixel group I of arbitrary shape that appears at different locations in two images I_1 and I_2 with a relative displacement of ΔX, ΔY. Let this pixel group I represent the only nonzero pixels in each image, thus the contribution of surrounding pixels to the following equations can be assumed to be zero. Consider now the sum of the product of the pixels and their respective X and Y locations in each image:

$$S_x^1 = \sum_j \sum_i I(i, j) X_{ij}^1$$

$$S_x^2 = \sum_j \sum_i I(i, j) X_{ij}^2.$$

In the second summation, the pixel locations can be represented as a displacement with respect to the first image. Thus,

$$S_x^2 = \sum_j \sum_i I(i, j)(X_{ij}^1 + \Delta X).$$

From these equations ΔX can be computed as:

$$\Delta X = \frac{S_x^2}{\sum_j \sum_i I(i, j)} - \frac{S_x^1}{\sum_j \sum_i I(i, j)}.$$

Similarly ΔY can be computed as:

$$\Delta Y = \frac{S_y^2}{\sum_j \sum_i I(i, j)} - \frac{S_y^1}{\sum_j \sum_i I(i, j)}.$$

The quantities

$$M_x = \frac{\sum_j \sum_i I(i, j) X_{ij}}{\sum_j \sum_i I(i, j)} \text{ and } M_y = \frac{\sum_j \sum_i I(i, j) Y_{ij}}{\sum_j \sum_i I(i, j)}$$

represent the first moment or the center of mass coordinates of the image. Thus, the translation displacement of a pixel group represented at different locations in two images can be computed as a difference in first moments of the two images, assuming all other pixel elements are zero in both images. Hence, precise displacement of a pixel

group in a set of images can be determined as long as it undergoes only pure displacement without any other changes in their values or distribution.

However, the binary maps of actual MRI images that need to be registered do not meet these ideal requirements due to several factors such as image noise, deformable motion of organs, and the presence of surrounding structures. As a result, the difference in first moments does not yield the exact displacement involved. Thus, robust processing involving exhaustive search for a match, such as using cross-correlation measure between the two images, becomes necessary. In our approach, we first use the first moment as a predictor to determine the neighborhood of the actual displacement. We then follow it by a cross-correlation method to refine the registration in the immediate vicinity with a small search range, thus saving high computational overhead associated with larger search regions that may be necessary otherwise.

Cross-correlation of two images $I_1(x,y)$ and $I_2(x,y)$ for a given displacement (i,j) is defined as:

$$R(i, j) = \frac{\sum_x \sum_y I_1(x, y) I_2(x - i, y - j)}{\sqrt{\sum_x \sum_y I_1^2(x, y)} \sqrt{\sum_x \sum_y I_2^2(x, y)}}$$

and is a measure of the goodness of registration between the two. Since I_1 and I_2 are binary, this simplifies to:

$$R(i, j) = \frac{\sum_x \sum_y I_1(x, y) I_2(x - i, y - j)}{\sqrt{\sum_x \sum_y I_1(x, y)} \sqrt{\sum_x \sum_y I_2(x, y)}}.$$

For implementation efficiency, we calculate the squared-correlation as:

$$R^2(i, j) = \frac{[\sum_x \sum_y I_1(x, y) I_2(x - i, y - j)]^2}{\sum_x \sum_y I_1(x, y) \sum_x \sum_y I_2(x, y)}.$$

We compute $R^2(i,j)$ for every possible pair (i,j) within the search region as guided by the motion of the center of the mass and pick the displacement which maximizes the squared correlation coefficient:

$$(\hat{i}, \hat{j}) = \arg\max_{(i,j)} R^2(i, j).$$

Implementation

The following steps describe the process flow of the method for registering the images using an automatic, pairwise, cross-correlation-based technique:

1) The user first identifies the region of interest to be registered by clicking on the organ of interest in any one image of the time-series. The algorithm uses this selected point to center a window and extracts the data to be used for cross-correlation matching. The size of the extracted window is preset and is based on the typical size of heart and kidneys observed in perfusion imaging. The default window size used in our experiments was 80 × 80 pixels. However, the user interface permits changing the window size if the organ of interest is too large or too small. The user must ensure that the chosen window is just large enough to encompass the organ of interest in all time frames. The 80 × 80 choice was sufficient in all experiments reported in this article.
2) The windowed data is next converted to binary form by thresholding. The threshold value used is computed from the pixel data itself and is set to the mean signal intensity in the windowed image. Since the threshold is computed independently for each image, it is insensitive to intensity changes due to contrast variations.
3) The first moment (or center of mass) of the windowed and thresholded data from two successive images is calculated and compared. The motion of the center of the mass yields the initial coarse estimate of motion and is used to set the boundaries of the roaming region over which the cross-correlation is evaluated. The roaming region is centered at the location of the center of mass and is 10 × 10 pixels wide. If the center of mass undergoes very large displacement between adjacent images (greater than 10 pixels), then the center of mass is discarded and the correlation search window is restricted to 10 × 10 pixels centered on the original image. This yields insensitivity to large intensity variations such as those occurring during arrival of contrast agents.
4) Cross-correlation between the two images is computed for every possible displacement of the second image within this search region. The optimal estimate of displacement is found by maximizing the squared cross-correlation within the search zone. The second image is then translated by the computed displacements to align it spatially with the first image.
5) This process is repeated for all pairs of images in the series.

The above algorithm is depicted as a flowchart in Fig. 1. The algorithm was implemented using IDL (Research Systems Inc., Boulder, CO) as part of a custom MRI Display and Analysis Tool (CINE tool). The implementation is platform-independent and has been tested on a Sun Ultra Sparc II workstation (Sun Microsystems, Sunnyvale, CA) and on Windows 2000 (Microsoft, Redmond, WA), both with 256 MB RAM. On the Windows platform, 10 images are registered per second using the automatic method. User interaction is limited to one click-point to identify the approximate position of the organ of interest in any one image. The user can also adjust the window size if necessary.

APPLICATIONS

Our method was validated on time-series MRI data involving organs that undergo significant motion during image acquisition such as cardiac and renal perfusion and BOLD

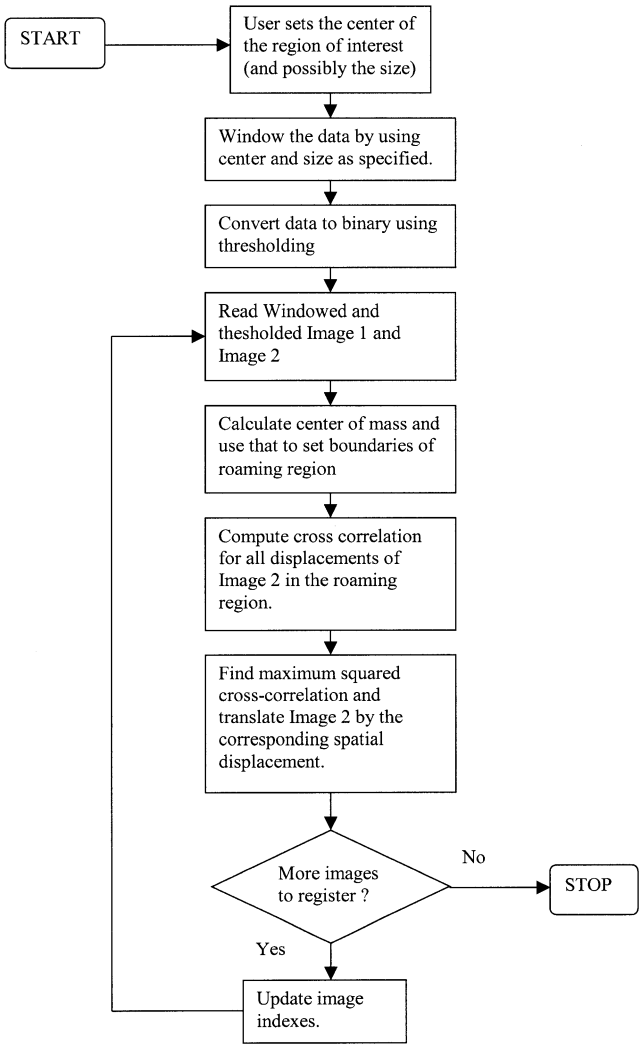

FIG. 1. Registration algorithm flowchart.

imaging. In these applications we observed that the method significantly reduced the misalignment of images, thus enhancing the usefulness of qualitative cine display of temporal course of events and accuracy of quantification from these time-series. The results for the three applications are summarized below.

Myocardial Perfusion

Data Acquisition

Ten patients were scanned under IRB-approved protocols using a GE Signa 1.5 T MRI system (GE Medical Systems, Waukesha, WI) with a high-performance gradient subsystem (40 mT/m, 150 T/m/sec). Between four and six first-pass perfusion image slices were collected every heartbeat during infusion of an exogenous contrast agent (Gd-DTPA). Images were collected over a 1–2-min period using a fast-gradient echo sequence (27) and patients were instructed to suspend breathing for a comfortable period and breathe normally thereafter. An illustrative perfusion image is shown in Fig. 2.

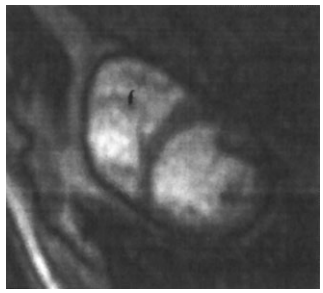

FIG. 2. Sample myocardial perfusion image.

Due to respiratory motion, the spatial location of the heart in the sequence of images undergoes large displacement (typically 5–10 pixels). This can be seen in Fig. 3a, where we show a section of the heart through a serial stack of the time sequence and the edge profile of left-ventricular myocardium can be seen (labeled "A"). We noticed that the predominant motion was in-plane translation due to the motion of the diaphragm. Small but noticeable rotational motion was also present in a few cases, which is not addressed by the current method.

Results

The motion occurring in these images before and after image registration was analyzed as follows. In each of the

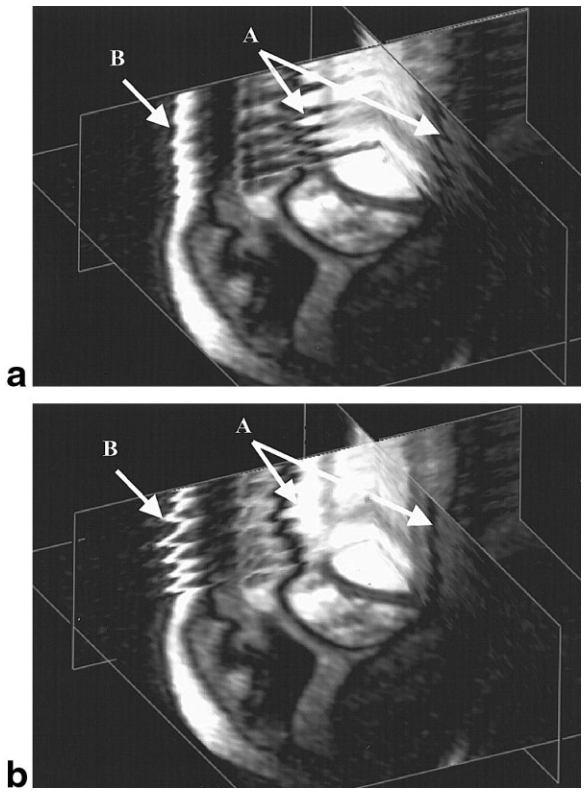

FIG. 3. Cut-plane sections through the time-series data, showing the profile of the structures under motion. Unregistered data (**a**), registered data (**b**). "A" depicts the profile of the myocardial edges and "B" depicts the chest wall profile.

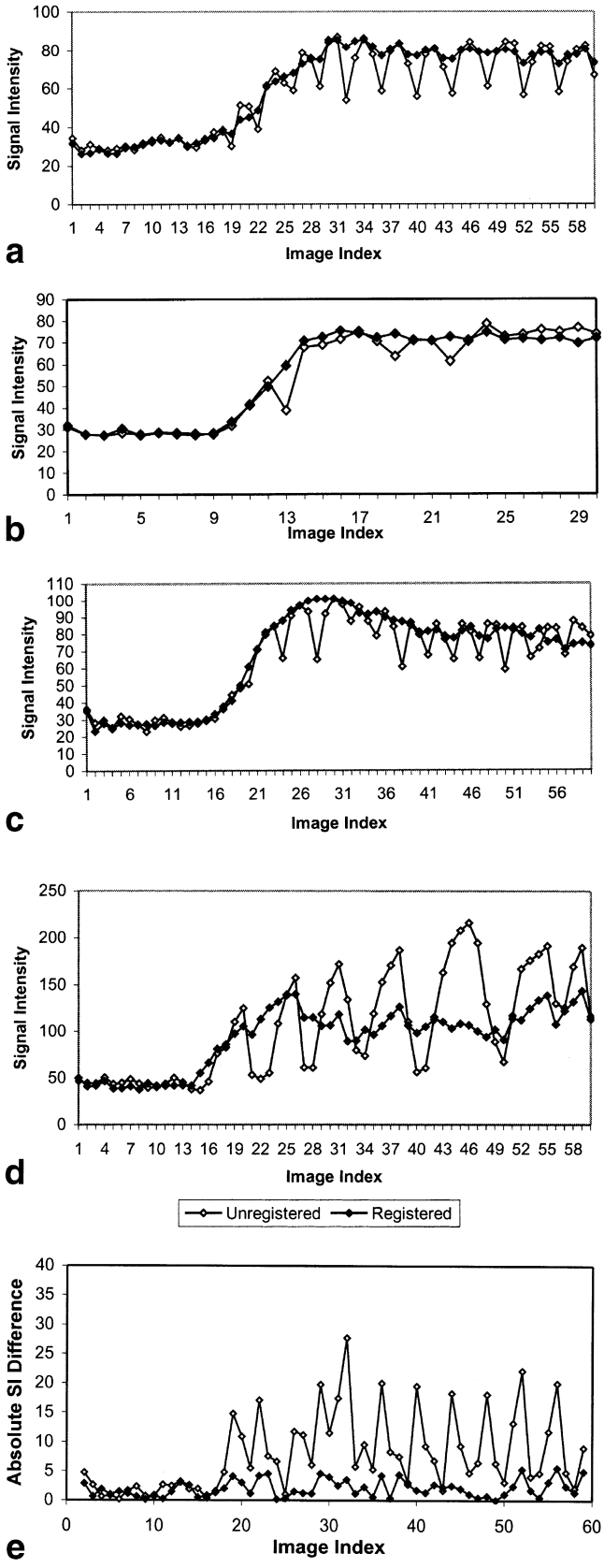

images, the anterior right-ventricular (RV) insertion point was manually identified as a landmark. Accuracy of registration was quantified by measuring the motion of this landmark between successive image pairs, both in unregistered and registered time-series.

A total of 433 images from 10 patients were analyzed. The mean motion in the original unregistered images was 3.32 pixels and the standard deviation was 2.68. After automatic registration (as described above), the mean motion was 0.27 pixels and the SD was 0.80. Thus, our proposed method yields more than a 10-fold reduction in registration error. The mean error if just the center of mass is used to estimate motion is 1.67 pixels. We compared the computational performance of using a simple cross-correlation-only technique with our proposed approach and obtained a speedup of 11.1 times compared to just a cross-correlation technique (28). An example is depicted in Fig. 3b, where we see that the temporal profile of myocardial edges (labeled "A") is more uniform than that in Fig. 3a. Note that in this application, as we chose the LV chamber to be the structure of interest that requires registration, the surrounding structures that were stationary prior to registration may now appear misaligned. This can be seen in the chest-wall area (labeled "B") in Fig. 3b. The importance of registration can be seen by comparing signal intensity vs. time curves for a small region of interest placed in the posterior lateral wall of the myocardium before and after automatic registration. We show curves from four subjects in Fig. 4a–d. Preregistration curves exhibit large variations particularly at later image indices due to breathing motion causing the region of interest to move in and out of tissue boundaries. In contrast, the postregistration curves are more uniform and characteristic of the true wash-in effect, which should permit a more representative estimation of subclinical perfusion indexes such as maximum upslope, time to peak enhancement, and contrast enhancement ratio. It should be noted that the postregistration curves also exhibit a small amount of variability, primarily due to the effects of through-plane motion not accounted for here. To quantify the variability of ROI signal intensities due to motion and to assess the impact of registration, we computed the absolute signal intensity difference between adjacent images for all time–intensity curves. Since the signal intensity is expected to vary rapidly during the upslope of the myocardial enhancement, we calculated the signal intensity difference as:

$$\text{Difference}(t) = \text{mag}[SI_{ROI\,t} - ((SI_{ROI\,t-1}) + (SI_{ROI\,t+1}))/2]$$

where $SI_{ROI\,t}$ is the mean signal intensity in the ROI in the image at time t. A difference plot for the curves in Fig. 4a

FIG. 4. Sample time–intensity curves from a small region of interest placed in the posterior lateral wall of the myocardium before and after registration for four subjects (**a–d**). The lines joined by empty symbols represent the curves before registration and the lines joined by filled symbols represent the curves after registration. **e:** The absolute signal intensity difference between adjacent images for the curves in **a** to characterize the variability in ROI signal values due to motion before and after registration.

is shown in Fig. 4e. On average, the absolute signal intensity difference was 6.6 ± 3.9 before registration and 2.9 ± 1.5 after registration ($P = 0.004$). Since breathing artifacts tended to be more common towards the end of the acquisition, as can be seen in Fig. 4a–d, we also performed this analysis on the last 20 images of each acquisition. For these images the absolute signal difference was 7.9 ± 4.7 before registration and 3.0 ± 1.9 after registration ($P = 0.002$). The maximum absolute signal intensity difference was 25.7 ± 15.5 before registration compared with 8.6 ± 6.1 after registration ($P < 0.001$). Thus, in summary, apparent image-to-image variability was 2–3 times worse on perfusion images preregistration. Automatic registration had significant benefits in defining the myocardial signal intensity–time curves more accurately.

It should be pointed out that by using manual registration subsequent to the automatic method, the residual error of 0.27 pixels can be removed and the images can be perfectly registered in the sense that the chosen landmark can be exactly aligned. Our experiments show that an image sequence comprising 50 frames can be automatically registered in 5 sec. We found that only 30 images out of the 433 studied required manual correction after automatic registration. As a result, manual postregistration correction could be performed in approximately 1 min, whereas a completely manual approach required approximately 10 min. This shows the substantial reduction in processing time achievable for registering large time-series datasets when using automatic registration in combination with manual correction vs. a fully manual approach.

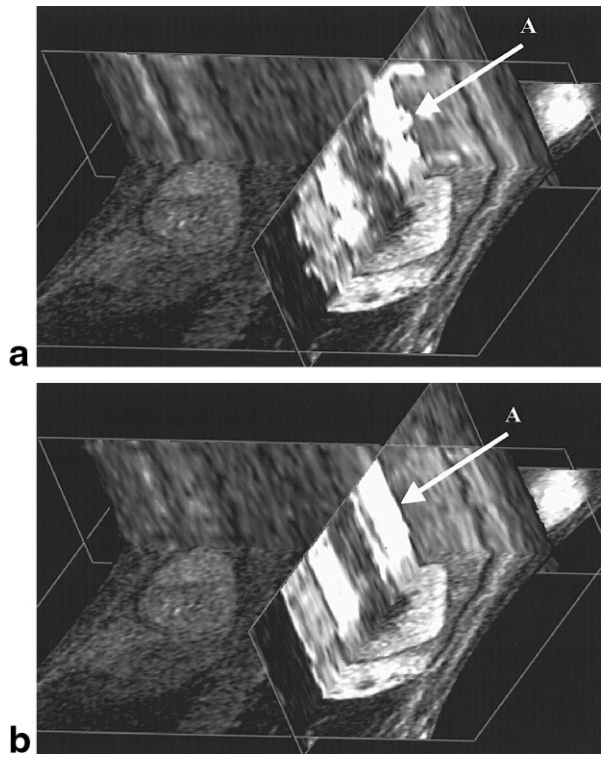

FIG. 6. Cut-plane sections through the time-series data, showing the profile of the structures under motion. Unregistered data (**a**), registered data (**b**). "A" depicts the profile of the renal edge.

Renal Perfusion

Data Acquisition

First-pass renal perfusion data was acquired using the technique reported in (29). Time-series data was obtained using an ungated, fast gradient-echo sequence and an image was acquired every 5 sec for a period of 1–2 min. Six patients were scanned under an IRB-approved protocol and the images were analyzed for motion before and after automatic registration.

Results

In all, 264 images from six patients were analyzed. The mean motion before registration was 3.75 pixels (SD = 3.02). After automatic registration, the mean motion was 0.27 pixels (SD = 1.53). The mean error if just the center of mass is used to estimate motion is 2.25 pixels. Figures 5, 6a,b, respectively, show an example of renal perfusion image, the profile of the unregistered data, and the profile after image registration. Dramatic improvement in the alignment of renal edge profile can be seen (labeled "A"). The time for automatic and manual processing was similar to that reported in Myocardial Perfusion above.

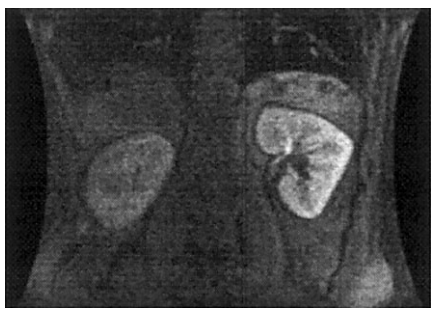

FIG. 5. Sample renal perfusion image.

Myocardial BOLD Imaging

Blood oxygenation level-dependent (BOLD) MRI has been applied to the human heart as a means of assessing perfusion reserve indexed by the change in transverse relaxation-time (T_2^*) under administration of a pharmacological stress agent, without the use of exogenous contrast agents (30). Just as in perfusion imaging, in order to accurately determine T_2^* changes it is important to correct for motion of the temporal data.

Data Acquisition

We analyzed five healthy subjects from a previously reported study comparing T_2^* changes in response to dipyridamole in healthy volunteers vs. hypertensive patients (31). Approximately 30 temporal image frames over rest and stress epochs were acquired using a breathheld technique. Corresponding to each image in this time series, we derived a composite T_2^* image, an extrapolated TE = 0 proton-density image, and the image corresponding to

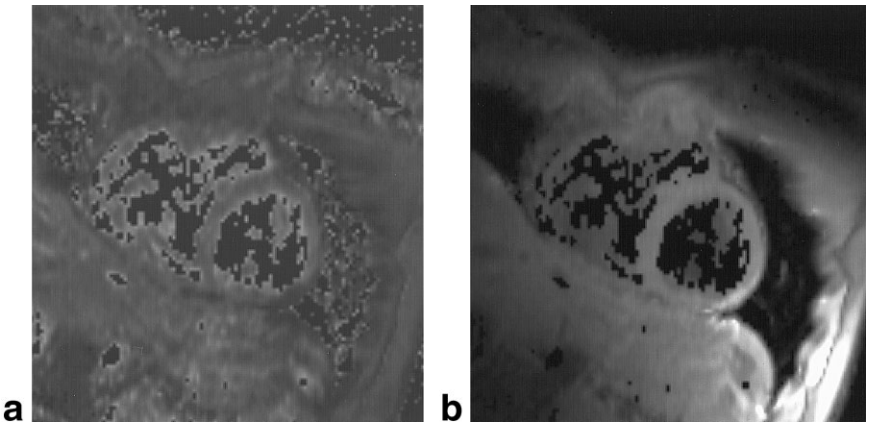

FIG. 7. **a:** Sample T_2^* image from a BOLD myocardial study. **b:** Corresponding extrapolated proton-density image.

the shortest TE value (31). The error in the registration algorithm was quantified from the displacement of the anterior RV insertion point between successive T_2^* images. Figure 7 shows an example of a T_2^* image and the corresponding extrapolated proton density image.

Results

Typical SNR of the underlying TE images used to generate T_2^* images ranged from approximately 40 (for the shortest TE) to 10 (for the longest TE) and the mean SNR of the composite T_2^* images was 4. The mean displacement of the RV insertion point for the five subjects in the unregistered images was 1.8 pixels. Our method was first directly applied to register these images, yielding a mean motion of 1.6 pixels after registration (11% improvement). The performance of the method was poor because the T_2^* images suffer from signal decay and lack the high-definition structures that aid the registration. In an alternate approach, we first registered the higher definition extrapolated TE = 0 images used as a template and then copied this registration to the underlying T_2^* data. By this method we reduced the motion to 0.6 pixels (67% improvement). This application highlights that in situations where the image quality is insufficient for accurate automatic registration, it may be possible to use co-registered synthetic images with higher contrast as templates, register them, and then apply the results to the underlying data for better performance. These registered images were used for physiological assessment of the BOLD effect in (32).

A summary of the results from each of the above three applications is shown in Table 1. A plot of the comparison of true motion, error from automatic registration, and error from center of mass alone is shown in Fig. 8 from all cardiac and renal perfusion subjects studied.

DISCUSSION

We have demonstrated a method that automatically registers time-series MRI data correcting for translational motion due to respiration or patient movement. The method was validated on datasets from cardiac perfusion, renal perfusion, and myocardial BOLD imaging. The proposed method is amenable to hardware implementation and can possibly be used to directly register images by the scanner reconstruction and postprocessing software itself. The current implementation relies on being guided by an initialization point centered in the organ of interest. This step can be automated by using the center of the field-of-view of the acquisition window. The size of the correlation window can also be determined empirically from the image pixel size.

As mentioned previously, we noticed no significant rotational component of motion of the organs in consideration in the planes of interest. However, the method can be adapted to perform rotational registration by the use of second-order moments, which are invariant under rotations.

Converting images to a binary representation by thresholding is the enabling component of this method in adapting routine cross-correlation-based image registration techniques for perfusion imaging applications. In perfusion imaging, the passage of contrast agent causes different organs to appear with increased signal intensity during the time-course. Thus, use of center of mass alone as an esti-

Table 1
Summary of Results

Application	No. of subjects (images)	Mean motion before reg. (in pixels)	Mean motion after auto reg. (in pixels)
Cardiac perfusion	10 (433)	3.32	0.27
Renal perfusion	6 (264)	3.75	0.27
Cardiac BOLD	5 (150)	1.80	0.60

mate of motion is prone to error since the effective image shape changes during the inflow and outflow of the agent. Our method is insensitive to these changes, as it is able to find the optimum cross-correlation match by searching in a restricted region of the original image and disregarding the large displacement of the center of mass. This is shown in Fig. 9, where we compare the motion of the center of the mass of the windowed-thresholded image with the final estimate of motion yielded by the method for one of the subjects from Myocardial Perfusion above. It can be seen that for a majority of the time points, the center of mass displacement tracks the final estimate of true motion of the image to a good approximation. The time points where there is a large difference between the two correspond to those time points when the contrast agent kinetics light up other organs within the correlation window, as shown by sharp changes in the image area profile. Thus, in addition to correctly identifying these situations and correcting for them, the method provides a way to detect the time-of-arrival of contrast-agent boluses. This has applications in perfusion image analysis and flow quantification.

Application of the technique to myocardial BOLD imaging reveals that in situations where the image SNR is inherently limited due to the physics (as in T_2^* images), it may be possible to synthesize higher-definition data (e.g., extrapolated proton-density images) and use them for increasing the accuracy of registration. The method can be used in a wide class of applications that deal with constructing parametric maps from underlying time-series data.

The overall goal of this study was to develop a technique for compensating motion, thus allowing automatic analysis and quantification of time-series data. External clinical measures will be required to determine whether the proposed registration methods affect the determination of and increase the validity of derived physiological parameters.

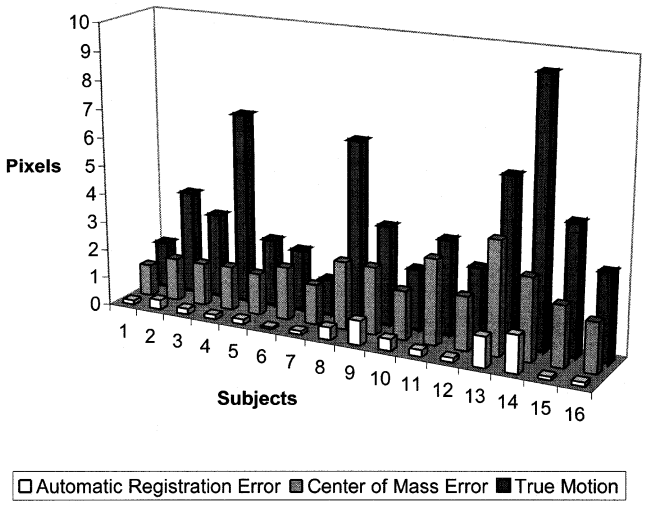

FIG. 8. Comparison of average true motion, automatic registration error, and error in center of mass across all subjects from cardiac and renal perfusion applications.

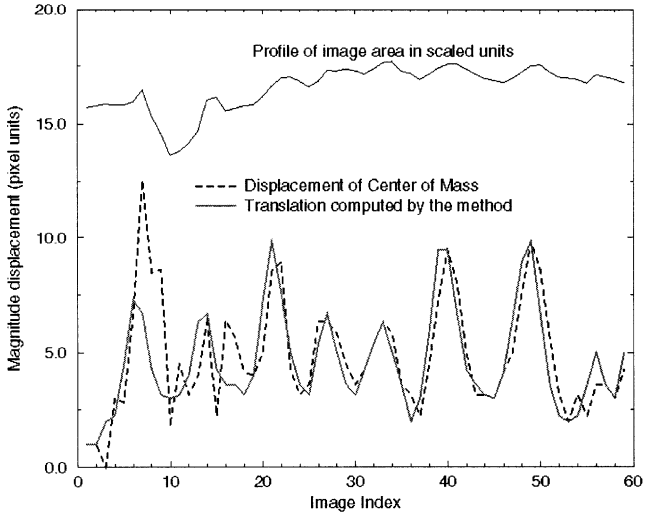

FIG. 9. Comparison of displacement of center of mass with the true translation computed by the method, in relation to the changing image area due to intensity variations caused by contrast agent flow.

REFERENCES

1. Atkinson DJ, Burstein D, Edelman RR. First-pass cardiac perfusion: evaluation with ultrafast MR imaging. Radiology 1990;174:757–762.
2. Wilke N, Jerosch-Herold M, Stillman AE, Kroll K, Teskos N, Merkle H, Parrish T, Hu X, Wang Y, Bassingthwaite J, Bache RJ, Ugurbil K. Concepts of myocardial perfusion imaging in magnetic resonance imaging. Magn Res Q 1994;10:249–286.
3. Cullen JHS, Horsfield MA, Reek CR, Cherryman GR, Barnett DB, Samani NJ. A myocardial perfusion reserve index in humans using first-pass contrast enhanced magnetic resonance imaging. J Am Col Cardiol 1999;33:1386–1394.
4. van den Elsen PA, Pol ED, Viergever MA. Medical image matching — a review with classification. IEEE Eng Med Biol 1993;3:26–39.
5. Alpert NM, Bradshaw JF, Kennedy D, Correia JA. The principal axes transformation — a method for image registration. J Nucl Med 1990;31: 1717–1722.
6. Venot A, Leclerc V. Automated correction of patient motion and gray values prior to subtraction in digitized angiography. IEEE Trans Med Imag 1984;3:179–186.
7. Woods RP, Cherry SR, Mazziotta JC. Rapid automated algorithm for aligning and re-slicing PET images. J Comput Assist Tomogr 1992;16: 620–633.
8. Junck L, Moen JG, Hutchins GD, Brown MB, Kuhl DE. Correlation methods for the centering, rotation, and alignment of functional brain images. J Nucl Med 1990;31:1220–1226.
9. de Castro E, Morandi C. Registration of translated and rotated images using finite Fourier transforms. IEEE Trans PAMI 1987;9:700–703.
10. Venot A, Devaux JY, Herbin M, Lebruchec JF, Dubertret L. An automated system for the registration and comparison of photographic images in medicine. IEEE Trans Med Imag 1988;7:298–303.
11. Boesecke R, Bruckner T, Ende G. Landmark based correlation of medical images. Phys Med Biol 1990;35:121–126.
12. Yang G, Burger P, Panting J, Gatehouse PD, Rueckert D, Pennel DJ, Firmin DN. Motion and deformation tracking for short-axis echo-planar myocardial perfusion imaging. Med Imag Anal 1998;2:285–302.
13. Bidaut LM, Vallee JP. Automated registration of dynamic MR images for the quantification of myocardial perfusion. J Magn Reson Imag 2001;13:648–655.
14. Gerig G, Kikinis R, Kuoni W, von Schultess GK, Kubler O. Semi-automated ROI analysis in dynamic MR studies. I. Image analysis tools for automated correction of organ displacements. J Comput Assist Tomogr 1991;15:725–732.
15. Fredrickson JO, Wegmuller H, Herfkens RJ, Pelc NJ. Simultaneous temporal resolution of cardiac and respiratory motion in MR imaging. Radiology 1995;195:169–175.

16. Anuta PF. Digital registration of multispectral video imagery. Soc Photo-Optic Instrum Eng J 1969;7:168–175.
17. Hibbard LS, Hawkins RA. Objective image alignment for 3-dimensional reconstruction of digital autoradiograms. J NeuroSci Meth 1988; 26:55–74.
18. Kvasnicka HM, Thiele J. 3D reconstruction of serial sections in light-microscopy. Pathologe 1995;19:128–137.
19. Studholme C, Hill DLG, Hawkes DJ. Automated 3D registration of magnetic resonance and positron emission tomography brain images by multiresolution optimization of voxel similarity measures. Med Phys 1997;24:25–35.
20. Maes F, Collignon A, Vandermeulen D, Marchal G, Suetens P. Multimodality image registration by maximization of mutual information. IEEE Trans Med Imag 1997;16:187–198.
21. Didon JP, Langevin F. Fast 3D registration of MR brain images using the projection correlation registration algorithm. Med Biol Eng Comput 1998;36:107–111.
22. Pratt WK. Correlation techniques of image registration. IEEE Trans Aero Elec Sys1974;10:353–358.
23. Barnea DI, Silverman HF. A class of algorithms for fast digital image registration. IEEE Trans Comput 1972;C-21:179–186.
24. Giele ELW, de Priester JA, Blom JA, den Boer JA, van Engelshoven JMA, Hasman A, Geerlings M. Movement correction of the kidney in dynamic MRI scans using FFT phase difference movement detection. J Magn Res Imag 2001;14:741–749.
25. Hu MK. Visual pattern recognition by moment-invariants. IRE Trans Inf Theory 1962;Feb:169–187.
26. Pitts W, McCulloch W. On how we know universals: the perception of auditory and visual forms. Bull Math Biophys 1947;9:127–147.
27. Ding S, Wolff SD, Epstein FH. Improved coverage in dynamic contrast-enhanced cardiac MRI using interleaved gradient-echo EPI. Magn Reson Med 1998;39:514–519.
28. Solaiyappan M, Gupta SN. Predictive registration of cardiac MR perfusion images using geometric invariants. In: Proc 8th Annual Meeting ISMRM, Denver, 2000. 1:37.
29. Slavin GS, Gupta SN, Choyke PL, Foo TKF. Rapid multi-slice renal perfusion MR imaging with simultaneous angiographic screening. In: Proc 10th Annual Meeting ISMRM, Honolulu, 2002. p 2370.
30. Li DB, Oellerich WF, Beck G, Gropler RJ. Assessment of myocardial response to pharmacological interventions using an improved MR imaging technique to estimate T2* values. AJR 1999;172:141–145.
31. Beache GM, Herzka DA, Boxerman JL, Post WS, Gupta SN, Faranesh AZ, Solaiyappan M, Bottomley PA, Weiss JL, Shapiro EP, Hill MN. Attenuated myocardial vasodilator response in patients with hypertensive hypertrophy revealed by oxygenation-dependent MRI. Circulation 2001;104:1214–1217.
32. Solaiyappan M, Beache GM, Gupta SN, Bottomley PA. A graphical approach for the analysis of myocardial BOLD Effect. In: Proc 9th Annual Meeting ISMRM, Glasgow, 2001. p 599.